Kramers-Kronig Optical OFDM for Bandlimited Intensity Modulated Visible Light Communications

Ruowen Bai, *Graduate Student Member, IEEE*, and Steve Hranilovic, *Senior Member, IEEE*

***Abstract*—Visible light communication (VLC) operates on optical intensity channels that are inherently limited in bandwidth. Though Kramers-Kronig (KK) receivers have been considered as a lower complexity alternative for coherent fiber optic communication (FOC) systems, in this paper we extend this concept to bandlimited IM/DD VLC channels and propose KK optical OFDM (KKO-OFDM). In KKO-OFDM the optical power of a low-cost LED is directly modulated by the double-sideband (DSB) squared modulus of a minimum phase single-sideband (SSB) signal. This results in a real-valued, non-negative and strictly bandlimited transmit signal which is suitable for VLC channels. At the receiver, the phase of the transmitted SSB signal is reconstructed via the KK relations. The required DC bias, average electrical signal-to-noise ratio (SNR), bit error rate (BER), and capacity are analyzed with approximate closed-forms and through simulation. Numerical results show that KKO-OFDM achieves the same spectral efficiency as the existing DC biased optical OFDM (DCO-OFDM), however, realizes approximately 1 dB optical SNR gain at a BER$= 10^{-4}$ while simultaneously having a small peak-to-average power ratio.**

***Index Terms*—Visible light communication, Light-fidelity (LiFi), Kramers-Kronig receiver, optical OFDM.**

I. Introduction

VISIBLE light communication (VLC) systems are emerging complementary links to radio due to the ubiquity of solid-state illumination as well as the availability of unregulated optical spectrum [1]–[6]. For a VLC system, a light-emitting diode (LED) is used as a transmitter and its optical intensity is modulated to carry information (i.e., intensity modulation (IM)). The receiver is typically a photodiode (PD) which produces an electrical current in proportion to the intensity of light (i.e., direct detection (DD)). Such IM/DD systems must drive the LED with a real-valued and non-negative electrical current signal, while maintaining a constraint on the average amplitude (i.e., intensity) [1]–[6].

The low-cost white LEDs employed in IM/DD VLC systems have a low-pass characteristic and have a typical modulation bandwidth of only several tens of MHz [7]. Orthogonal frequency division multiplexing (OFDM) has been considered as a candidate modulation scheme for such systems due to its high spectral efficiency, resistance to inter-symbol interference (ISI), simple one-tap equalization and extensive usage in wired and wireless broadband communications [6]–[11]. Direct current (DC) biased optical OFDM (DCO-OFDM) is a popular OFDM scheme for IM/DD systems due to its simplicity and high spectral efficiency. In order to generate a transmittable signal, a real output is guaranteed by imposing Hermitian symmetry in frequency domain and a DC bias is added to ensure non-negativity. If a fixed DC bias is selected, there is a risk of clipping the DCO-OFDM signals resulting in out-of-band (OOB) distortion which is not bandlimited [12]. Alternatively, the DC bias can be varied symbol-by-symbol to ensure non-negativity, resulting in no OOB distortion [13]. However, this method can cause flickering and is not suitable for VLC systems that are required to provide stable illumination. Asymmetrically clipped optical OFDM (ACO-OFDM) is another popular scheme for VLC systems, in which only odd subcarriers are modulated [8]. Using the anti-symmetric property of such signals, the negative parts are clipped at zero directly without any loss of information. However, OOB clipping distortion still exists due to sharp transition caused by this zero clipping [12]. Alternative approaches have also been considered, namely spectrally factorized optical OFDM (SFO-OFDM) [14] which considers the generation of bandlimited IM signals directly through the autocorrelation of a complex data sequence to guarantee non-negativity. However, the demodulation requires high computational complexity for a practical SFO-OFDM system with many subcarriers.

In related coherent fiber-optic communication (FOC) systems, data are transmitted in both the amplitude and the phase of an electric field of a laser. Recently, low complexity receivers for such FOC coherent links have been proposed which can recover both the amplitude and phase from measurements of the intensity using a PD at the receiver [15]–[19]. These systems require that the transmitted complex signal is a minimum phase waveform and rely on the Kramers-Kronig (KK) relations to recover the phase [15].

In this paper, we extend the application of the KK relations to develop a strictly bandlimited IM/DD optical OFDM modulation format termed as *KK Optical*-OFDM (KKO-OFDM). In KKO-OFDM, a minimum phase single-sideband (SSB) complex signal is employed to carry information and its squared modulus is utilized to directly modulate the optical power emitted from a low-cost LED. Mathematically, the squared modulus

Manuscript received June 4, 2021; revised August 11, 2021; accepted September 2, 2021. Date of publication September 8, 2021; date of current version November 16, 2021. This work was presented in part at the 2021 IEEE North American School of Information Theory. This work was supported by the Natural Sciences & Engineering Research Council of Canada. *(Corresponding author: Steve Hranilovic.)*

The authors are with the Department of Electrical and Computer Engineering, McMaster University, Hamilton, ON L8S 4K1, Canada (e-mail: bair4@mcmaster.ca; hranilovic@mcmaster.ca).

Color versions of one or more figures in this article are available at https://doi.org/10.1109/JLT.2021.3110661.

Digital Object Identifier 10.1109/JLT.2021.3110661

of an SSB signal is necessarily non-negative and strictly bandlimited and has no OOB clipping distortion as compared to conventional DCO- and ACO-OFDM. At the receiver, a PD is used to detect the received optical power and the KK relations are used to infer the phase information to reconstruct the original SSB signal. Unlike related work on coherent FOC channels, where the KK relations are used to reconstruct the phase of an electric field, here the squared modulus of an SSB signal is used to directly modulate the optical power emitted by the white LEDs in a VLC system and the KK relations are used to infer the phase of this SSB signal at the receiver. Compared to recent work in VLC optical single side-band OFDM (SSB-OFDM) [7], KKO-OFDM does not require upsampling and up-conversion at the transmitter, resulting in less complexity, which is attractive to VLC systems employing low-cost simplicity LEDs.

The paper provides a design guide for KKO-OFDM for VLC channels. A theoretical bit error rate (BER) is derived which shows a small gap to the simulated results and thus can be employed to evaluate the performance conveniently. The capacity of KKO-OFDM is analysed and a small gap is found compared to capacity bounds of IM/DD OWC channels in existing literature. The computation complexity of KKO-OFDM is comparable to DCO-OFDM at the transmitter, however requiring greater complexity at the receiver. Monte Carlo simulation results show that KKO-OFDM is more power efficient compared to DCO-OFDM and LACO-OFDM for a bandlimited VLC systems achieving a 1.0 dB gain over bandlimited DCO-OFDM and 1.4 dB gain over bandlimited LACO-OFDM at BER$= 10^{-4}$. The peak-to-average power ratio (PAPR) of KKO-OFDM signals is shown to be smaller than DCO-OFDM and LACO-OFDM, indicating the increased robustness of KKO-OFDM to LED nonlinear transfer characteristics.

The balance of the paper is organized as follows. Section II describes bandlimited IM/DD optical OFDM schemes and introduces the transceiver for KKO-OFDM. KKO-OFDM design and signal analysis are presented in Section III. Numerical results are analysed in Section IV. Finally, conclusions are drawn in Section V.

II. Bandlimited KK Optical-OFDM Definition

A. Conventional Bandlimited Optical OFDM

For comparison and completeness, in this subsection we define two conventional strictly bandlimited optical OFDM approaches. A continuous, finite energy signal $s(t)$ is defined as bandlimited to frequency range $[-B, B]$ if the support of its Fourier transform is limited to $[-B, B]$.

In DCO-OFDM with N subcarriers, the 0-th and $N/2$-th subcarriers are set to zero with data symbols modulated onto the remaining subcarriers. Hermitian symmetry, i.e., $X_k = X^*_{N-k}$, is imposed on each OFDM symbol to ensure the output of inverse fast Fourier transform (IFFT), x_n, a real-valued signal [8]. Assuming the available bandwidth of the LED is B, consider constructing the strictly bandlimited data bearing signal $x(t)$ via Nyquist-Shannon interpolation as [21]

$$x_{\text{DCO}}(t) = \underbrace{\sum_{n=-\infty}^{\infty} x_n \text{sinc}\left(2Bt - n\right)}_{x(t)} + D_{\text{DCO}} \tag{1}$$

where $\text{sinc}(\zeta) = \sin(\pi\zeta)/(\pi\zeta)$, $x(t)$ is the data-bearing signal and D_{DCO} is a DC bias added to satisfy the non-negativity constraint. To improve power efficiency, consider adaptively setting the DC bias per OFDM frame as the minimum required to ensure non-negativity [13]

$$D_{\text{DCO}} = -\min\{x(t)\}. \tag{2}$$

In ACO-OFDM, data symbols are only modulated onto the odd subcarriers with even subcarriers set to zero while imposing Hermitian symmetry in the frequency domain. The resulting output of IFFT x_n is anti-symmetric and clipping the negative parts to zero results in no loss of information leading to [8]

$$x_{\text{clip},n} = \frac{1}{2}x_n + \frac{1}{2}|x_n|,\ 0 \le n \le N-1 \tag{3}$$

where $\frac{1}{2}|x_n|$ is clipping distortion only onto even subcarriers.

Similar to DCO-OFDM in (1), consider constructing a bandlimited signal with samples $x_{\text{clip},n}$ using Nyquist-Shannon interpolation leading to $x_{\text{clip}}(t)$. Though $x_{\text{clip},n} \ge 0$, after interpolation, $x_{\text{clip}}(t)$ may no longer satisfy the non-negativity constraint, hence a sufficiently large DC bias must be added to $x_{\text{clip}}(t)$ as in [12], [13] leading to

$$x_{\text{ACO}}(t) = x_{\text{clip}}(t) + D_{\text{ACO}} \tag{4}$$

where $D_{\text{ACO}} = -\min\{x_{\text{clip}}(t)\}$.

To enhance the spectral efficiency, LACO-OFDM simultaneously transmits the sum of L layers of ACO-OFDM signals in the time domain [22]. These ACO-OFDM layers employ disjoint sets of subcarriers, with each layer satisfying an anti-symmetric property. Define similarly, $x_{\text{L,clip},n}$ as sum of samples of the L layers of ACO-OFDM and $x_{\text{L,clip}}(t)$ as the bandlimited signal arising from Nyquist-Shannon interpolation. To ensure non-negativity a sufficiently large DC bias, $D_{\text{LACO}} = -\min\{x_{\text{L,clip}}(t)\}$, is adaptively added to each LACO-OFDM symbol, resulting in a non-negative bandlimited signal $x_{\text{LACO}}(t)$.

B. KKO-OFDM Transmitter

The transmitter block diagram for KKO-OFDM with N subcarriers is shown in Fig. 1(a). For convenience, assume N is a power of 2. The bits to be transmitted are first mapped to quadrature amplitude modulation (QAM) symbols. These QAM constellation symbols are modulated onto subcarriers with index number of $k = 1, \ldots, N/2 - 1$ with remaining subcarriers set to zero to form the SSB frequency-domain symbol as

$$\mathbf{X} = \left[0, X_1, X_2, X_3, \ldots, X_{N/2-1}, \underbrace{0, \ldots, 0}_{N/2 \text{ zeros}}\right]. \tag{5}$$

Notice that different from DCO-OFDM, KKO-OFDM does not require Hermitian symmetry.

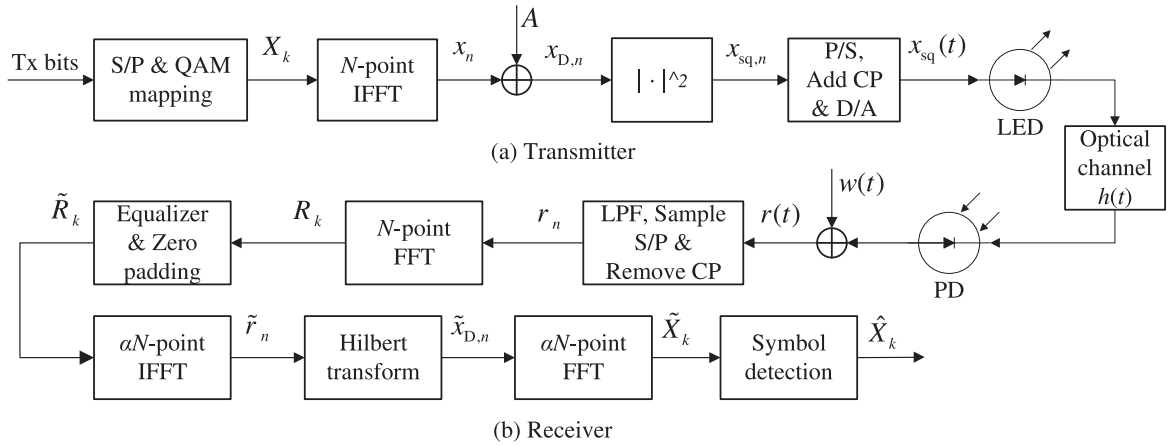

Fig. 1. Transmitter (a) and receiver (b) block diagrams for KKO-OFDM.

The frequency-domain symbol $\mathbf{X}$ is fed into an N-point IFFT module leading to time-domain signal $\mathbf{x}$, of which the n-th element is given by

$$x_n = \frac{1}{\sqrt{N}} \sum_{k=0}^{N-1} X_k \exp\left(j\frac{2\pi}{N}nk\right),\ 0 \le n \le N-1 \quad (6)$$

where x_n is a complex-valued signal.

Consider adding a real DC bias $A > 0$ to the SSB-signal x_n to ensure that resulting $x_{\mathrm{D},n}$ is a minimum phase waveform [15], [16], given by

$$x_{\mathrm{D},n} = x_n + A. \quad (7)$$

An SSB signal is a minimum phase waveform for which all roots are outside the unit circle [15]. In this work, in order to avoid flickering in VLC systems, A is set as a constant. The selection of A is discussed at length in Section III-B.

For a minimum phase signal such as $x_{\mathrm{D},n}$, the phase and the natural logarithm of its amplitude form a Hilbert transform pair [15]. Thus, only intensity of $x_{\mathrm{D},n}$ need be transmitted over the channel without any loss of information. The phase can be recovered completely from the measurements of the intensity at the receiver. Thus, define the driving signal for the LED as

$$x_{\mathrm{sq},n} = \|x_{\mathrm{D},n}\|^2 \quad (8)$$

where $\|\cdot\|$ denotes the magnitude of a complex value.

Notice that while $x_{\mathrm{D},n}$ is a complex-valued single-sideband signal, $x_{\mathrm{sq},n}$ is a real-valued, double-sideband (DSB) signal with support over discrete frequency indices $\{0, \ldots, N-1\}$ [15].

After parallel-to-serial (P/S) and padding a CP, the transmitted intensity signal $x_{\mathrm{sq}}(t)$ is formed using Nyquist-Shannon interpolation as

$$x_{\mathrm{sq}}(t) = \sum_{n=-\infty}^{\infty} x_{\mathrm{sq},n}\mathrm{sinc}(2Bt - n). \quad (9)$$

Notice that $x_{\mathrm{sq}}(t)$ is real, strictly bandlimited to frequencies $[-B, B]$ and $\forall t$, $x_{\mathrm{sq}}(t) \ge 0$ since it arises as the magnitude square of a single-sideband signal [14]. That is, $x_{\mathrm{sq}}(t)$ is a strictly bandlimited signal satisfying the non-negativity constraint without the need of clipping or additional bias.

Unlike coherent FOC systems where the electric field of a laser is modulated by a complex-valued signal [15], [16], [18], here KKO-OFDM produces a real-valued, non-negative, bandlimited signal $x_{\mathrm{sq}}(t)$ as LED drive current to directly modulate the optical power of the light emitted by an LED for VLC systems.

The average optical power of KKO-OFDM signal is proportional to the mean of $x_{\mathrm{sq}}(t)$, which is given by

$$P_{\mathrm{o}} = \mathrm{E}\{x_{\mathrm{sq}}(t)\} = \mathrm{E}\{(x_{\mathrm{r},n} + A)^2 + x_{\mathrm{i},n}^2\} = \mathrm{E}\{\|x_n\|^2\} + A^2 \quad (10)$$

where $x_{\mathrm{r},n}$ and $x_{\mathrm{i},n}$ are real and imaginary parts of x_n, respectively and $\mathrm{E}\{\cdot\}$ denotes expectation.

C. KKO-OFDM Receiver

The KKO-OFDM receiver block diagram is shown in Fig. 1(b). A PD is utilized to convert the received optical intensity into a photocurrent, which is assumed proportional to the received instantaneous optical power. The optical bandwidth of the PD response, B_{PD} is generally much greater than the bandwidth of an LED, i.e., $B_{\mathrm{PD}} \gg B$. The detected photocurrent, $r(t)$, is contaminated by high-intensity shot noise and thermal noise and is given by [2], [20], [26]

$$r(t) = h_{\mathrm{VLC}}(t) \otimes x_{\mathrm{sq}}(t) + w(t) \quad (11)$$

where $h_{\mathrm{VLC}}(t)$ is impulse response (IR) for the VLC channel. The combination thermal noise and high-intensity shot noise, $w(t)$, can be well modelled as signal-independent additive white Gaussian noise (AWGN) [2], [20], [26].

The front end of the receiver consists of an ideal low pass filter (LPF) to B Hz followed by Nyquist rate sampling, and removal of the cyclic prefix (CP). Equalization is performed in frequency domain by a single complex multiplication in each frequency bin after an N-point FFT. Since r_n is real, its DFT R_k has a Hermitian symmetry. Thanks to this Hermitian symmetry, only $N/2$ complex-valued multiplications are required to implement the one-tap equalization. As is conventional in KK receivers for

FOC systems, up-sampling is required for subsequent steps [15]. Let $\alpha \geq 1$ denote the up-sampling factor, i.e., αN samples per symbol. Here, up-sampling is accomplished by zero padding in frequency domain in prior to performing an αN-point IFFT to yield signal $\widetilde{r}_n$.

Recall that for a minimum phase waveform, the phase and the natural logarithm of amplitude form a Hilbert transform pair [15], [16]. Define $\widetilde{x}_{\mathrm{D},n}$ as a minimum phase waveform with phase $\widetilde{\phi}_n$ so that $\|\widetilde{x}_{\mathrm{D},n}\|^2 = \|\widetilde{r}_n\|$ which can be shown to always exist [15]. Hence, $\widetilde{\phi}_n$ can be estimated through the Hilbert Transform block in Fig. 1(b) as

$$\widetilde{\phi}_n = \mathcal{H}\left(\log\left(\sqrt{\|\widetilde{r}_n\|}\right)\right) \tag{12}$$

where $\mathcal{H}$ denotes the Hilbert transform. Subsequently, $\widetilde{x}_{\mathrm{D},n}$ is estimated as

$$\widetilde{x}_{\mathrm{D},n} = \sqrt{\|\widetilde{r}_n\|}\exp\{j\widetilde{\phi}_n\}. \tag{13}$$

Taking the DFT of $\widetilde{x}_{\mathrm{D},n}$, an estimate of X_k can be obtained as

$$\widetilde{X}_k = \frac{1}{\sqrt{\alpha N}}\sum_{n=0}^{\alpha N-1}\widetilde{x}_{\mathrm{D},n}\exp\left(-j\frac{2\pi}{\alpha N}nk\right). \tag{14}$$

Finally, symbol detection is employed to detect the modulated QAM symbols as

$$\widehat{X}_k = \arg\min_{X\in\Omega_X}\|X - \widetilde{X}_k\|,\ k = 1,\ldots,N/2-1 \tag{15}$$

where Ω_X denotes the constellation set of symbols.

III. KKO-OFDM Design & Analysis

A. Spectral Efficiency

The spectral efficiency is defined as the transmitted bit rate divided by bandwidth usage. Assume N_{CP} is the length of CP used and constellation size is M for each sub-carrier. For KKO-OFDM, $N/2-1$ subcarriers out of N are employed to modulate QAM symbols, hence the spectral efficiency is

$$\Upsilon_{\mathrm{KKO}} = \frac{N/2-1}{N+N_{\mathrm{CP}}}\log_2(M)\ \text{ bits/s/Hz}. \tag{16}$$

Note that (16) is also the spectral efficiency of DCO-OFDM [8].

For ACO-OFDM, the spectral efficiency is given by [8]

$$\Upsilon_{\mathrm{ACO}} = \frac{N/4}{N+N_{\mathrm{CP}}}\log_2(M)\ \text{ bits/s/Hz} \tag{17}$$

while the spectral efficiency of LACO-OFDM with L layers is given by [11], [22]

$$\Upsilon_{\mathrm{LACO}} = \left(1-\frac{1}{2^L}\right)\frac{N/2}{N+N_{\mathrm{CP}}}\log_2(M)\ \text{ bits/s/Hz}. \tag{18}$$

Based on comparison among these OFDM schemes, the spectral efficiencies of DCO- and KKO-OFDM are the highest while ACO-OFDM is the smallest. As L increases, the spectral efficiency of LACO-OFDM approaches that of DCO- and KKO-OFDM.

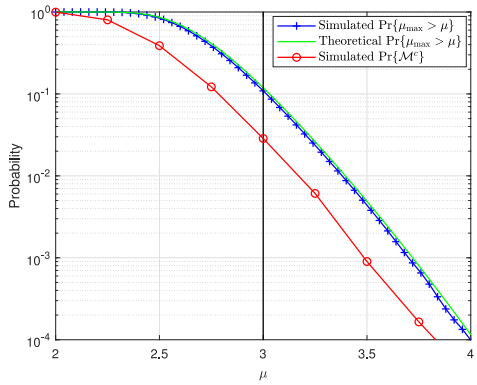

Fig. 2. CCDF of $\mu_{\max}$ for KKO-OFDM signals ($N = 1024$ and 16-QAM).

B. Selection of DC Bias A

Given that KKO-OFDM only transmits the squared modulus of the data signal, $x_{\mathrm{D}}(t)$ must be a minimum phase in order to recover the phase exactly. From [17], $x_{\mathrm{D}}(t)$ is minimum phase if and only if the DC bias A is large enough to ensure that the winding number of the trajectory of $x_{\mathrm{D}}(t)$ in complex plane is zero. Define $\mathcal{M}$ as the event that $x_{\mathrm{D}}(t)$ is minimum phase. A more tractable sufficient condition for a given signal $x_{\mathrm{D}}(t)$ to be minimum phase is to set $A \geq A_{\max}$ where [15]

$$A_{\max} = \max_t\|x(t)\|. \tag{19}$$

Define $\mathcal{S}$ as the event that for a fixed bias A the sufficient condition holds, i.e., that $A \geq A_{\max}$ for a random selection $x(t)$. In the following, the likelihood of $\mathcal{S}$ will be used to lower bound the probability of $\mathcal{M}$ when using a fixed value of DC bias A.

For a given OFDM symbol, (19) can be approximated as

$$A_{\max} \approx \max_{0\leq n\leq N-1}\|x_n\|. \tag{20}$$

According to central limit theorem (CLT) [24], the real and imaginary parts of x_n are distributed as $x_{\mathrm{r},n} \sim \mathcal{N}(0,\sigma_x^2/2)$ and $x_{\mathrm{i},n} \sim \mathcal{N}(0,\sigma_x^2/2)$ where $\sigma_x^2 = \mathrm{E}\{\|x_n\|^2\}$. In addition, $x_{\mathrm{r},n}$ and $x_{\mathrm{i},n}$ are statistically independent resulting in the amplitude $\|x_n\|$ following a Rayleigh distribution. The complementary cumulative distribution function (CCDF) of $A_{\max}$ is thus

$$\begin{aligned}F_{A_{\max}}(a) &= \Pr\{A_{\max} > a\} = 1 - \Pr\{\cap_{\forall n}\{\|x_n\| \leq a\}\}\\ &= 1 - \left(1-\exp\left(-\left(\frac{a}{\sigma_x}\right)^2\right)\right)^N.\end{aligned} \tag{21}$$

Notice that $F_{A_{\max}}(A) = \Pr\{\mathcal{S}^c\}$ where the superscript 'c' indicates the set complement. Noting the form of (21), for readability, define $\mu_{\max} = A_{\max}/\sigma_x$ where

$$F_{\mu_{\max}}(\mu) = \Pr\{\mu_{\max} > \mu\} = 1 - \left(1-\exp\left(-\mu^2\right)\right)^N. \tag{22}$$

Consider selecting a fixed bias $A = \mu\sigma_x$ for some μ in order to ensure that the resulting $x_{\mathrm{D}}(t)$ is minimum phase with a sufficiently high probability. Fig. 2 presents $\Pr\{\mathcal{S}^c\}$ using the closed-form CCDF (22) based on the sufficient condition (19) as well as $\Pr\{\mathcal{M}^c\}$ using the definition in Section II-B and simulated for $N = 1024$ and 16-QAM.

Notice that the closed-form on $\Pr\{\mathcal{S}^c\}$ aligns well with simulated results and can be used as a convenient, but loose, upper bound on $\Pr\{\mathcal{M}^c\}$. For example, for $\mu = 3$, $\Pr\{\mathcal{M}^c\} = 0.03$ while $F_{\mu_{\max}}(3) = 0.11$. Interestingly, numerical results in Section IV-B indicate KKO-OFDM with $\mu = 3$ can achieve $\mathrm{BER} < 10^{-4}$ when employing 16-QAM. That is, the proposed KKO-OFDM receiver is able to correctly detect the transmitted symbols even when $x_{\mathrm{D}}(t)$ is *not* a minimum phase. Increasing A will cause smaller $\Pr\{\mathcal{M}^c\}$ at the expense of reduced optical power efficiency. Therefore, the selection of A, and equivalently μ, must be carefully tuned to balance optical power efficiency with the probability of $x_{\mathrm{D}}(t)$ being a minimum phase. The theoretical bound from (22) serves as a useful starting point for the selection of μ.

From (10),

$$P_{\mathrm{o}} = (\mu^2 + 1)\sigma_x^2. \tag{23}$$

Dimming of the illumination of the VLC-enabled luminaire is closely related to the average optical power P_{o}. The values of μ and of σ_x^2 can be carefully set to achieve a specific dimming target. From Section IV-B2, the optimal value of μ is fixed for a specific constellation size. Hence, $\sigma_x^2 = P_{\mathrm{o}}/(\mu^2 + 1)$ is carefully adjusted to satisfy the required dimming target.

Define the optical signal-to-noise ratio (OSNR) as [5], [6]

$$\mathrm{OSNR} = \frac{P_{\mathrm{o}}}{\sigma_w}. \tag{24}$$

C. Effective Average Electrical SNR

In order to obtain insight on the performance of KKO-OFDM, in this subsection an analytical estimate of the end-to-end electrical SNR is computed under the assumption of high OSNR, which is typical in many VLC applications [5], [25], [26]. An additional assumption of this analysis is that a sufficiently large bias A is added so that $x_{\mathrm{D},n}$ is minimum phase.

Consider rewriting the received signal in (12) as

$$\|\widetilde{r}_n\| = \left(\|x_{\mathrm{D},n}\|^2\right)\left(\|1 + 2v_n\|\right) \tag{25}$$

where

$$v_n = \frac{w_n}{2\|x_{\mathrm{D},n}\|^2}\ , \quad \|x_{\mathrm{D},n}\| > 0. \tag{26}$$

Substituting (25) into (12) gives

$$\widetilde{\phi}_n = \phi_n + \phi_{\mathrm{e},n} \tag{27}$$

where ϕ_n is the phase of $x_{\mathrm{D},n}$ and $\phi_{\mathrm{e},n}$ is the error in phase estimation given by

$$\phi_{\mathrm{e},n} = \mathcal{H}\left(\log\left(\sqrt{\|1 + 2v_n\|}\right)\right). \tag{28}$$

Substituting (25) and (27) into (13) gives

$$\begin{aligned}\widetilde{x}_{\mathrm{D},n} &= \|x_{\mathrm{D},n}\|\sqrt{\|1 + 2v_n\|}\exp\{j(\phi_n + \phi_{\mathrm{e},n})\} \\ &= x_{\mathrm{D},n}\sqrt{\|1 + 2v_n\|}\exp\{j\phi_{\mathrm{e},n}\}.\end{aligned} \tag{29}$$

When OSNR is large, $\|v_n\| < \epsilon$, for small real ϵ, with a high probability, and $\phi_{\mathrm{e},n}$ in (28) is equivalently small such that symbols can be detected successfully. Hence, using a first-order Taylor series approximation yields

$$\widetilde{x}_{\mathrm{D},n} \approx x_{\mathrm{D},n}\left(1 + v_n\right)\exp\{j\phi_{\mathrm{e},n}\} = x_{\mathrm{D},n} + \widetilde{w}_n \tag{30}$$

where $\widetilde{w}_n$ is an equivalent additive noise given by

$$\begin{aligned}\widetilde{w}_n &= x_{\mathrm{D},n}\left(\left(\exp\{j\phi_{\mathrm{e},n}\} - 1\right) + v_n\exp\{j\phi_{\mathrm{e},n}\}\right) \\ &\approx x_{\mathrm{D},n}\left(j\phi_{\mathrm{e},n} + v_n(1 + j\phi_{\mathrm{e},n})\right) \\ &= x_{\mathrm{D},n}\left(v_n + j\phi_{\mathrm{e},n}\left(1 + v_n\right)\right).\end{aligned} \tag{31}$$

From (28), using the first-order Taylor series approximation of the argument gives

$$\phi_{\mathrm{e},n} \approx \mathcal{H}\left(v_n\right). \tag{32}$$

Substituting (32) into (31) gives

$$\widetilde{w}_n \approx x_{\mathrm{D},n}\left(v_n + j\mathcal{H}\left(v_n\right)\left(1 + v_n\right)\right). \tag{33}$$

Hence, at high OSNR, the average power of noise can be approximated as

$$\begin{aligned}P_{\widetilde{w}} &= \mathrm{E}\{\|\widetilde{w}_n\|^2\} = \mathrm{E}\left\{\|x_{\mathrm{D},n}\|^2\left(v_n^2 + \mathcal{H}^2\left(v_n\right)\left(1 + v_n\right)^2\right)\right\} \\ &\approx \mathrm{E}\left\{\|x_{\mathrm{D},n}\|^2 v_n^2\right\} + \mathrm{E}\left\{\|x_{\mathrm{D},n}\|^2\mathcal{H}^2\left(v_n\right)\right\}.\end{aligned} \tag{34}$$

Given that typically $A \gg \|x_n\|$ (to ensure $x_{\mathrm{D},n}$ is minimum phase) and w_n is independent of $x_{\mathrm{D},n}$, v_n in (26) can be approximated as

$$v_n \approx \frac{w_n}{2A^2} = \frac{\mu^2 + 1}{2\mu^2}\frac{w_n}{P_{\mathrm{o}}}. \tag{35}$$

Substituting (35) into (34) gives

$$\begin{aligned}&P_{\widetilde{w}} = \\ &\frac{\left(\mu^2 + 1\right)^2\sigma_w^2}{4\mu^4 P_{\mathrm{o}}} + \frac{\left(\mu^2 + 1\right)^2\mathrm{E}\left\{\mathcal{H}^2\left(w_n\right)\right\}}{4\mu^4 P_{\mathrm{o}}} \overset{(a)}{=} \frac{\left(\mu^2 + 1\right)^2\sigma_w^2}{2\mu^4 P_{\mathrm{o}}}.\end{aligned} \tag{36}$$

where (a) arises since the Hilbert transform changes only the phase in the frequency domain, and the power remains the same, thus $\mathrm{E}\{\mathcal{H}^2(w_n)\} = \mathrm{E}\{w_n^2\} = \sigma_w^2$.

An underlying assumption of this analysis is that $\widetilde{x}_{\mathrm{D},n}$ and $x_{\mathrm{D},n}$ are minimum phase SSB signals. Hence $\widetilde{w}_n$ is an SSB signal according to (30). Let $\widetilde{W}_k$ denote the DFT of $\widetilde{w}_n$. Following Parseval's theorem, the electrical power of the signal and equivalent noise at each frequency bin can be approximated as

$$P_{\widetilde{W}} = \mathrm{E}\{\|\widetilde{W}_k\|^2\} = 2\mathrm{E}\{\|\widetilde{w}_n\|^2\} = 2P_{\widetilde{w}}. \tag{37}$$

and

$$P_{\mathrm{X}} = \mathrm{E}\{\|X_k\|^2\} = 2\sigma_x^2 = \frac{2P_{\mathrm{o}}}{\mu^2 + 1}. \tag{38}$$

Notice that in general $\widetilde{w}_n$ is dependent on the signal $x_{\mathrm{D},n}$ via (31). However, in practice and as shown in [23], after the FFT at the receiver in Fig. 1 the resulting time-domain signal-dependent noise is well approximated as being signal-independent. Hence, the average electrical SNR at each subcarrier can be estimated as

$$\mathrm{SNR}_{\mathrm{e}} = \frac{P_{\mathrm{X}}}{P_{\widetilde{W}}} \approx \frac{2\mu^4}{\left(\mu^2 + 1\right)^3}\frac{P_{\mathrm{o}}^2}{\sigma_w^2} = \frac{2\mu^4}{\left(\mu^2 + 1\right)^3}\mathrm{OSNR}^2. \tag{39}$$

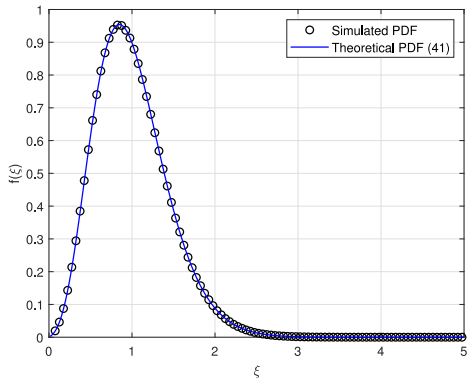

Fig. 3. Theoretical and simulated PDF of KKO-OFDM signal with QAM symbols ($\mu = 3$ and $P_{\rm o} = 1$, $M = 16$, $N = 1024$).

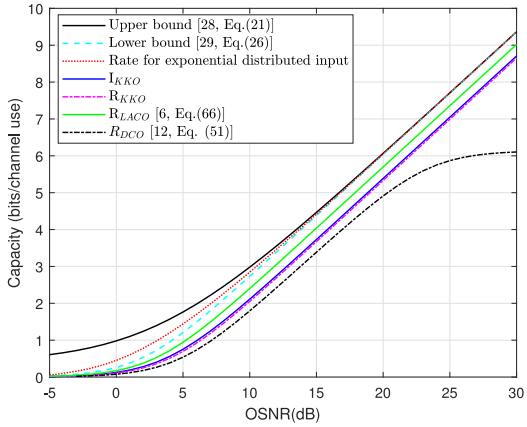

Fig. 4. Capacity bounds on data rate of KKO-OFDM ($\mu = 3$).

The BER of KKO-OFDM can thus be estimated as [31], [32],

$$\text{BER} \approx \frac{4(\sqrt{M}-1)}{\sqrt{M}\log_2 M} Q\left(\sqrt{\frac{6\mu^4}{(\mu^2+1)^3(M-1)}\text{OSNR}}\right) \tag{40}$$

where M is the rectangular QAM constellation size.

D. Capacity Analysis

Assuming $x_{\mathrm{r},n}$ and $x_{\mathrm{I},n}$ are accurately modelled as independent and Gaussian distributed, notice that $x_{\mathrm{sq},n} = (x_{\mathrm{r},n} + A)^2 + x_{\mathrm{i},n}^2$ follows a (scaled) noncentral chi-squared distribution with two degrees of freedom [27] and has probability density function (PDF)

$$f(\xi) = \frac{1}{\sigma_x^2} \exp\left\{-\frac{\mu^2\sigma_x^2 + \xi}{\sigma_x^2}\right\} I_0\left(\sqrt{\frac{4\mu^2\xi}{\sigma_x^2}}\right),\ \xi > 0 \tag{41}$$

where $I_\nu(y) = (y/2)^\nu \sum_{j=0}^{\infty} \frac{(y^2/4)^j}{j!\Gamma(\nu+j+1)}$ is a modified Bessel function of the first kind and $\Gamma(z)$ is the gamma function [27]. In the special case of $\mu = 0$, $f(\xi)$ is exponential. The theoretical and simulated PDF of KKO-OFDM signal with uniformly selected 16-QAM constellation points are depicted in Fig. 3. It can be seen the theoretical PDF follows closely the simulated PDF.

The capacity of the bandlimited average amplitude-constrained IM/DD channel can be lower bounded by the mutual information between $x_{\mathrm{sq},n}$ and r_n denoted as I_{KKO}

$$I_{\mathrm{KKO}} = h(r_n) - h(r_n|x_{\mathrm{sq},n}) = h(r_n) - h(w_n) \tag{42}$$

where $h(\cdot)$ denotes the differential entropy of a continuous random variable. The PDF of r_n can be calculated by convolving the PDF of $x_{\mathrm{sq},n}$ in (41) with the Gaussian noise distribution of w_n. The resulting I_{KKO} in (42) can thus be obtained numerically, though there is no closed-form is available.

On the other hand, a closed-form estimate of the information rate can be computed using the approximation for electrical SNR in (39) and Shannon's famous capacity expression for the AWGN channel [21].

Since the approximation in (39) relates the optical power constraint to an electrical power constraint, the resulting KKO-OFDM system can be treated as $N/2-1$ parallel independent complexed-valued AWGN channels or $N-2$ real-valued AWGN channels with an electrical SNR, SNR_{e} according to (39). The resulting estimate on the information rate of KKO-OFDM is

$$R_{\mathrm{KKO}} = \frac{1}{2}\log\left(1 + \frac{2\mu^4}{(\mu^2+1)^3}\text{OSNR}^2\right) \text{ bits/channel use} \tag{43}$$

for large N.

Fig. 4 presents the information rate of KKO-OFDM versus OSNR for bandlimited IM/DD channels with an average amplitude constraint. Additionally, an upper bound on the capacity of discrete-time IM/DD OWC channels [28] and lower bounds (using the entropy power inequality, exponential input distribution and LACO-OFDM [6]) are added as benchmarks. Notice that these bounds apply only to discrete-time IM/DD channels and do not simultaneously consider non-negativity and a strict bandwidth constraint.

The lower bound on the capacity of bandlimited IM/DD channels via I_{KKO} is close to the closed-form approximation R_{KKO} at each specific value of OSNR for $\mu = 3$. There is a gap between the information rate of KKO-OFDM and the bounds on the capacity of the discrete-time IM/DD OWC channel. This is not surprising given that KKO-OFDM is by construction bandlimited and earlier bounds are computed for discrete-time channels, which do not consider an explicit bandwidth limit. Indeed, discrete-time IM/DD channels can be made compatible with bandlimited channels via the Nyquist-Shannon interpolation formula at the expense of requiring an additional, and often large, DC bias as discussed in Section II-A and shown numerically in Section IV. The information rate of DCO-OFDM with a fixed DC bias $D_{\mathrm{DCO}} = 3\sigma_x$ is also presented in Fig. 4 according to (51) [12]. Due to the fixed bias, clipping distortion is unavoidable and results in a saturated rate in the high OSNR regime [12]. Notice that R_{KKO} is greater than R_{DCO} and the gain of KKO-OFDM over DCO-OFDM increases with OSNR.

E. Computational Complexity Analysis

At the transmitter, KKO-OFDM requires only a single N-point IFFT module, which is same as DCO-OFDM. The computational complexity of the transmitter is thus $\mathcal{O}(N \log_2\ N)$ [4]. In LACO-OFDM, L-IFFT modules are needed for L layers, resulting in a complexity of $(2 - 1/2^{L-1})\mathcal{O}(N \log_2\ N)$ [22]. Hence, DCO- and KKO-OFDM transmitters are less complex than LACO-OFDM, which makes them more suitable for low-cost LED luminaries in VLC systems.

At the receiver, DCO-OFDM requires an N-point FFT module, resulting in a computational complexity of $\mathcal{O}(N \log_2\ N)$ [4]. LACO-OFDM is demodulated recursively and the complexity can be estimated as $(5 - 1/2^{L-3})\mathcal{O}(N \log_2\ N)$ [22]. KKO-OFDM requires digital up-sampling, which employs an N-point FFT module and an αN-point IFFT module. Additionally, KKO-OFDM requires an additional Hilbert transform module, which can be achieved in frequency domain using an αN-point FFT module and an αN-point IFFT module [15]. In addition, an αN-point FFT is used before symbol detection. Hence, in total, the computational complexity can be estimated as $\mathcal{O}(\alpha N \log_2(\alpha N))$. Indeed the receiver of KKO-OFDM is more complex that DCO-OFDM, however, given the availability of computational resources at mobile receivers this complexity may be acceptable given the achieved gains quantified in the next section.

IV. Numerical Results

A. Bandlimited Optical OFDM and KKO-OFDM Waveforms

Examples time-domain waveforms for bandlimited IM/DD DCO-, ACO-, and KKO-OFDM are shown in Fig. 5 where the average optical power of all signals are normalized to unity.

Fig. 5(a) shows an example of DCO-OFDM time-domain waveform, from which it can be seen that all samples of DCO-OFDM $x_n + D_{\text{DCO}}$ fall onto $x_{\text{DCO}}(t)$ after Nyquist-Shannon interpolation using (1). Similarly, Fig. 5(b) shows an ACO-OFDM waveform where the minimum bias D_{ACO} is added to avoid clipping of the bandlimited Nyquist-Shannon interpolated signal (4).

Fig. 5(c) shows the KKO-OFDM time-domain waveform where $\mu = 3$. All samples of KKO-OFDM $x_{\text{sq},n}$ fall onto the signal $x_{\text{sq}}(t)$ constructed via Nyquist-Shannon interpolation using (9). In addition, $x_{\text{sq}}(t)$ is a non-negative and strictly bandlimited signal falling into $[-B,\ B]$. This result arises directly since the squared magnitude of a complex SSB signal is necessarily real, non-negative and remains bandlimited in $[-B,\ B]$. The bandlimited signal, $x_{\text{sq}}(t)$ is completely determined by the samples spaced $1/(2B)$ seconds apart [21].

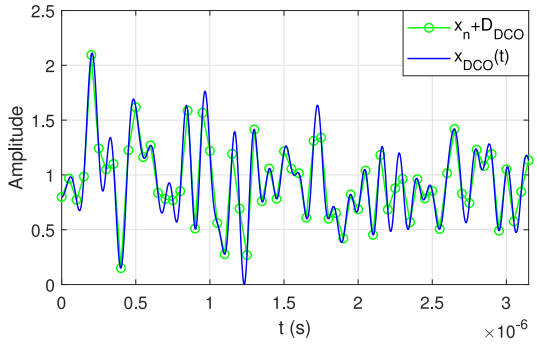

(a) Bandlimited DCO-OFDM

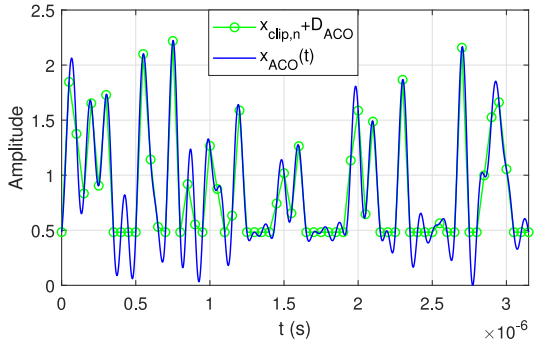

(b) Bandlimited ACO-OFDM

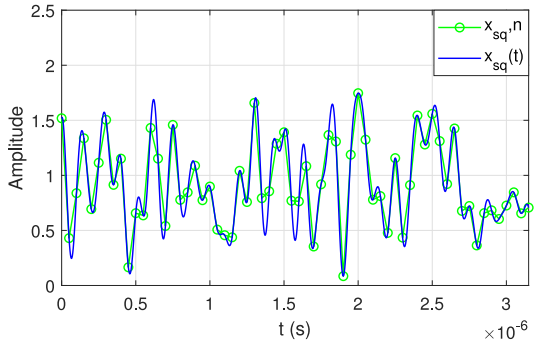

(c) KKO-OFDM

Fig. 5. Signals of DCO-, ACO-, and KKO-OFDM with/without Nyquist-Shannon interpolation normalized to have unit optical power ($N = 64$, $M = 16$ and $B = 10$ MHz).

B. BER Performance

In the case of line-of-sight (LOS) VLC links, and to aid in comparing with earlier work, a good model is to consider a flat channel response [8]. In the following, and without loss of generality, channel is assumed flat in the band of interest and the DC gain between the transmitter and receiver is assumed to be unity [8]. The number of subcarriers are set to $N = 1024$ and QAM constellations with gray labelling are employed. The bandwidth is set to $B = 10$ MHz in all simulations.

1) BER Versus α: The BER performance of KKO-OFDM for different values of up-sampling factor α is shown in Fig. 6, in which 16-QAM and $\mu = 3$ are used. It can be seen that the BER performance of KKO-OFDM improves and approaches the theoretical BER as α increases. From (12), notice that though $x_{\text{sq}}(t)$ is bandlimited, $\log(x_{\text{sq}}(t))$ is not necessarily bandlimited. As the up-sampling factor α increases, more information about $\log(x_{\text{sq}}(t))$ is collected and improved BER performance is achieved. However, increasing the up-sampling factor comes at the expense of increasing the computational complexity. From Fig. 6, the performance of the KKO receiver saturates at $\alpha = 4$ and small gains are available for further increases in α. Hence,

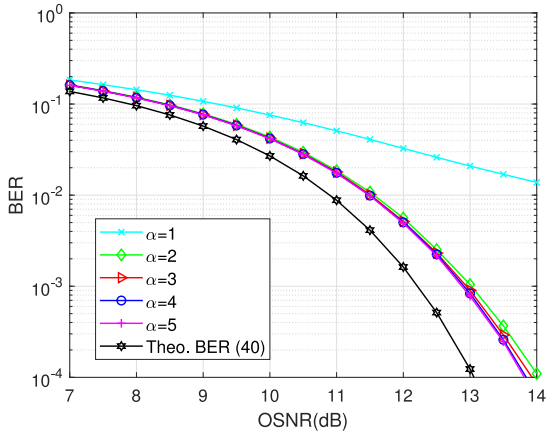

Fig. 6. BER performance of KKO-OFDM for different values of up-sampling factor with $\mu = 3$.

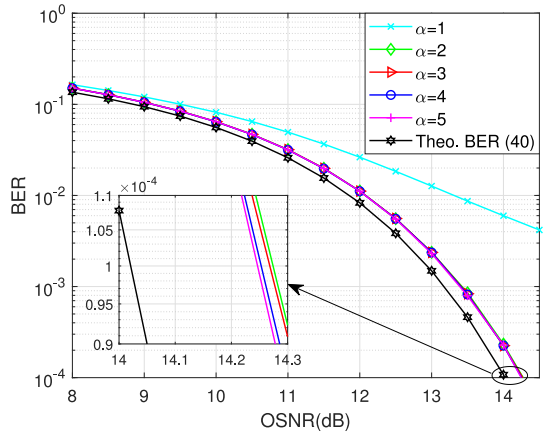

Fig. 7. BER performance of KKO-OFDM for different values of up-sampling factor with $\mu = 4$.

$\alpha = 4$ is employed to balance performance versus complexity in subsequent simulations.

Notice that the theoretical BER is loose at higher OSNRs. This gap arises primarily due to the fact that the theoretical BER given by (40) is based on a first-order Taylor series approximation, which holds only for large A and $x_{\mathrm{D}}(t)$ remaining a minimum phase signal. Additionally, limited oversampling results in inaccuracies in the logarithmic (12) and exponential (13) operations which are nonlinear. Thus, the theoretical BER according to (40) can be treated as an estimate of performance.

Similar KKO-OFDM BER results are shown in Fig. 7 with $\mu = 4$ for various α. In this case, the theoretical BER approximation in (40) is much tighter to the numerical results. This can be explained by the fact that when μ is large so too is A and the first-order Taylor series approximations used to compute (40) are more accurate. Notice also that for $\mu = 4$, the BER curves saturate for smaller values of α as compared to the case $\mu = 3$ illustrated in Fig. 6. This is because the first-order Taylor series approximation for the log of the received signal is more accurate as μ and equivalently A increases. Thus, increasing μ and A will cause power inefficiency while allowing for a decrease in

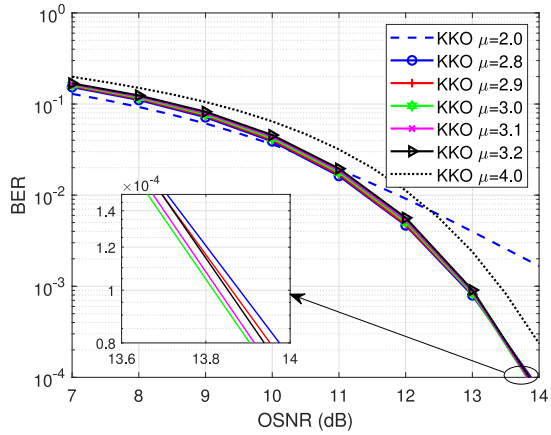

Fig. 8. BER performance of KKO-OFDM for different values of μ ($M = 16$ and $\alpha = 4$).

TABLE I
OPTIMAL μ FOR BER=10^{-4} OVER CONSTELLATION SIZES

M-QAM	4	16	64	128	256
Optimal μ	2.7	3.0	3.3	3.4	3.4

α leading to a decrease computational complexity. Therefore, there exists a trade-off between α and μ.

2) BER Versus μ: Fig. 8 presents the BER performance of KKO-OFDM for different values of μ using 16-QAM and $\alpha = 4$. Notice from Fig. 2 that $\mu \approx 3$ ensures that $x_{\mathrm{D},n}$ is minimum phase with high probability. As seen in the figure, if $\mu = 2$, $x_{\mathrm{D},n}$ is minimum phase with $\Pr\{\mathcal{M}\} = 0.004$ which dominates the overall BER regardless of OSNR. However, when $\mu = 4$, $x_{\mathrm{D},n}$ is minimum phase with high probability at the expense of reduced optical power efficiency (39) due to conservatively large choice of A resulting in worse BER performance than the case with $\mu = 3$.

Thus, $\mu = 3$ is used as the starting point to search for the optimal value for each OSNR for each constellation employed. Table I presents the optimal values of μ for various QAM constellations which minimize the OSNR required to achieve a BER$= 10^{-4}$. Notice that the optimal value of μ also increases with the order of QAM formats. For normalized constellations, the minimum distance decreases as the constellation size increases requiring a higher likelihood of $x_{D,n}$ being minimum phase to meet the SNR requirements at a given BER. Therefore, the optimal value of μ increases slightly as the order of QAM format increases.

In all cases, the values remain near $\mu = 3$ and balance the impact of increases P_{o} in (23) with the likelihood that the transmitted waveform is not minimum phase. The values of μ in Table I were found through extensive simulations are used in subsequent simulations.

3) Received Constellations: The received scatter plot of constellation points is shown in Fig. 9, where the OSNR$= 18$ dB, $\alpha = 4$ and 1000 OFDM symbols are simulated. Notice that the individual constellation points are easily discernible. In practice,

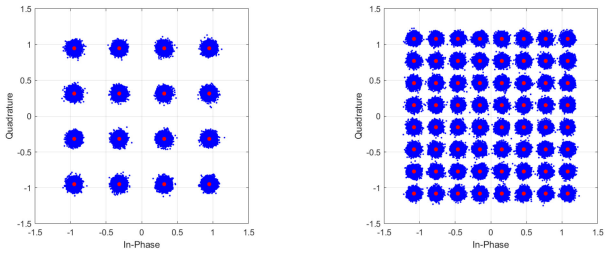

(a) 16-QAM (b) 64-QAM

Fig. 9. Scatter constellation plots of KKO-OFDM.

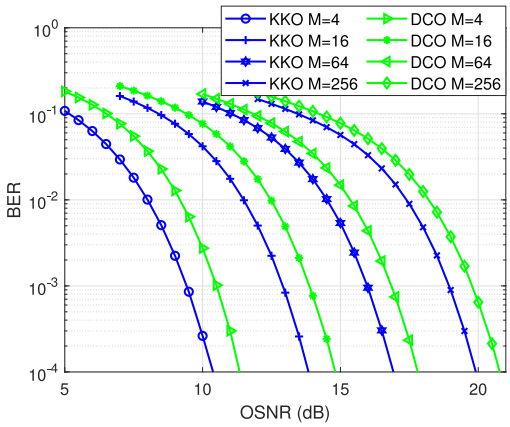

Fig. 10. BER comparison between KKO-OFDM and DCO-OFDM at the same constellation size and hence spectral efficiency (μ selected according to Table I).

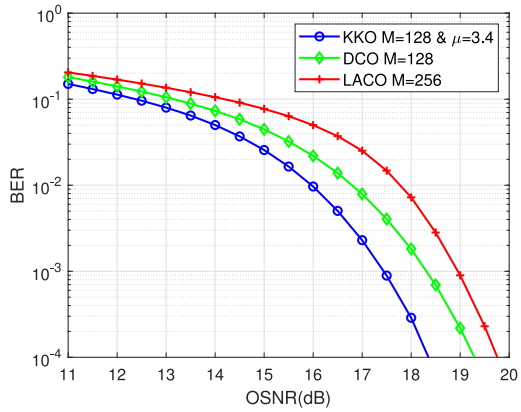

Fig. 11. BER comparison between KKO-OFDM, DCO-OFDM and LACO-OFDM at a spectral efficiency of 3.5 bits/s/Hz.

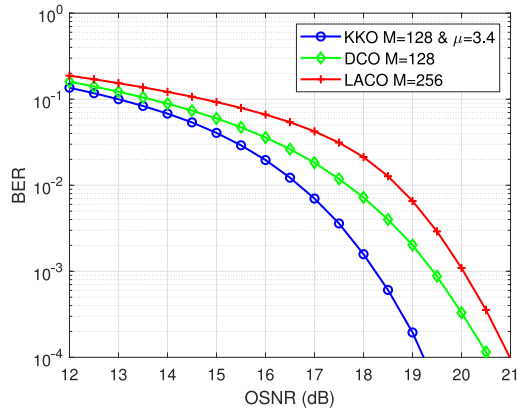

Fig. 12. BER comparison between KKO-OFDM, DCO-OFDM and LACO-OFDM under a VLC LPF channel at a spectral efficiency of 3.5 bits/s/Hz.

SNRs in VLC channels often operation and OSNRs significantly exceeding 18 dB [25].

4) BER Comparison: Fig. 10 presents the BER comparison between KKO-OFDM and DCO-OFDM operating the same spectral efficiency. Notice that both KKO- and DCO-OFDM have the same spectral efficiency for a given M. In particular, constellation sizes of $M = 4,\ 16,\ 64$ and 256 are employed yielding spectral efficiencies of $\Upsilon_{\text{KKO}} = 1,\ 2,\ 3$ and 4 bits/s/Hz, respectively. It can be seen that KKO-OFDM outperforms DCO-OFDM at these four spectral efficiencies at BER$= 10^{-4}$. Compared to DCO-OFDM, KKO-OFDM achieves about 1.0 dB OSNR gain at BER$= 10^{-4}$.

Notice that KKO-OFDM modulates a SSB signal and constrains its energy to signal carriers only, while DCO-OFDM modulates DSB signal requiring Hermitian symmetry. Additionally after Nyquist-Shannon interpolation, by construction there exist no negative peaks in KKO-OFDM. However, the large negative peaks in DCO-OFDM require a comparably large DC bias to meet the non-negativity constraint leading to optical power inefficiency.

A BER comparison between KKO-OFDM, DCO-OFDM and LACO-OFDM all operating at the same spectral efficiency of 3.5 bits/s/Hz is shown in Fig. 11. For KKO-OFDM and DCO-OFDM, 128-QAM is utilized while for LACO-OFDM, the number of layers is set to $L = 3$, and 256-QAM is utilized. It can be seen that KKO-OFDM achieves the best BER performance at the BER of 10^{-4} and achieves about 1.0 dB and 1.4 dB OSNR gains compared to DCO-OFDM and LACO-OFDM respectively.

5) BER in a VLC Lowpass Channel: In this section, BER performance of KKO-OFDM is evaluated in a VLC lowpass dispersive channel, which includes line-of-sight (LOS) path and diffuse reflections. The impulse response of this channel is well estimated by a close-form function as [2]

$$h_{\text{VLC}}(t) = H_{\text{DC}} \frac{\tau_0^6}{(t+\tau_0)^7} u(t) \tag{44}$$

where channel DC gain H_{DC} is assumed to be unity without loss of generality, $u(t)$ is the unit step function, $\tau_0 = 12\sqrt{11/13}\tau_{\text{rms}}$, and τ_{rms} is root-mean-square (rms) delay spread typically assumed to be 10 ns [2]. Here, the sampling rate to simulated the impulse response $h(t)$ is set to 60 MHz.

Fig. 12 presents BER comparison between KKO-OFDM, DCO-OFDM and LACO-OFDM in the lowpass VLC channel at the same spectral efficiency of 3.5 bits/s/Hz. For simplicity, a zero forcing equalizer is employed, which only requires $N/2$ complex-valued multiplications as discussed in Section II-C. It is apparent the proposed receiver in this paper can successfully demodulate KKO-OFDM under a VLC lowpass dispersive

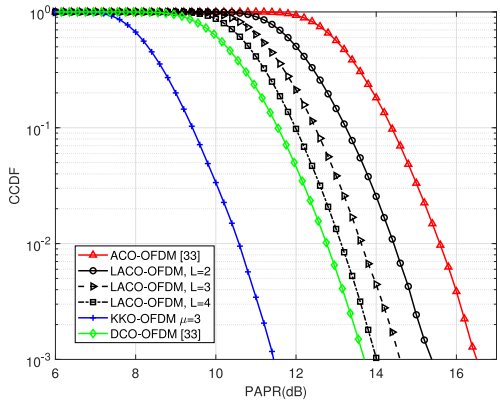

Fig. 13. PAPR comparison between KKO-OFDM, DCO-OFDM and LACO-OFDM ($N = 1024$).

channel. When BER$= 10^{-4}$, KKO-OFDM achieves a 1.3 dB and 1.8 dB optical gains compared to DCO-OFDM and LACO-OFDM with $L = 3$, respectively.

C. PAPR Performance

The CCDF comparison of PAPR for KKO-OFDM, DCO-OFDM and LACO-OFDM is shown in Fig. 13, where $N = 1024$ subcarriers is assumed. For ACO-OFDM and DCO-OFDM, the CCDF of PAPR is calculated using [33] while the CCDF of PAPR in LACO-OFDM is evaluated by simulation [6], [11]. For KKO-OFDM, $\mu = 3$ is used. It is worth noting that increasing μ will decrease PAPR, however it may degrade the BER performance.

As can be seen, the PAPR CCDF of KKO-OFDM is significantly lower than other approaches. In particular, at a CCDF value of 10^{-3}, the PAPR of KKO-OFDM is 2.3 dB and 5.1 dB smaller than DCO-OFDM and ACO-OFDM, respectively. This more compact PAPR distribution for KKO-OFDM suggests that it is more robust in the presence of nonlinear LED transfer characteristics.

V. Conclusions

In this paper, KKO-OFDM is introduced which produces an inherently real-valued, non-negative amplitude and strictly bandlimited signal well suited to IM/DD VLC systems. Relying on the KK relations, KKO-OFDM modulates an SSB signal and requires no Hermitian symmetry. Indeed, KKO-OFDM is the first inherently bandlimited IM/DD modulation format suitable for lowpass optical wireless channels. Unlike earlier work in optical fiber channels where the KK relations are used to retrieve the phase of a coherent laser emission, here we extend the use of the KK relations to develop an IM/DD system suited to bandwidth constrained VLC systems.

Numerical results are aligned well with analysis and show that KKO-OFDM outperforms DCO-OFDM and LACO-OFDM when operating at the same spectral efficiency and with a strict bandwidth limitation. We present a design guide for the selection of parameters for KKO-OFDM as well as closed-form approximations for the resulting electrical SNR and achievable information rates for the first time explicitly taking into account bandlimited channels. Numerical results show that an optical power gain of 1 dB over DCO-OFDM and 1.4 dB gains over LACO-OFDM are readily obtainable. On a low pass VLC channel, KKO-OFDM was able to realize a larger gain of 1.3 dB in optical SNR over DCO-OFDM. As an additional benefit, the PAPR distribution of KKO-OFDM signal is significantly more compact than DCO- and LACO-OFDM indicating an improved resilience to LED nonlinear characteristics.

Our future investigations include experimental demonstrations of this approach in realistic VLC channels.

References

[1] L. Hanzo, H. Haas, S. Imre, D. O'Brien, M. Rupp, and L. Gyongyosi, "Wireless myths, realities, and futures: From 3G/4G to optical and quantum wireless," *Proc. IEEE*, vol. 100, no. *Centennial Special Issue*, pp. 1853–1888, May 2012.

[2] J. M. Kahn and J. R. Barry, "Wireless infrared communications," *Proc. IEEE*, vol. 85, no. 2, pp. 265–298, Feb. 1997.

[3] A. A. Purwita, M. D. Soltani, M. Safari, and H. Haas, "Terminal orientation in OFDM-based LiFi systems," *IEEE Trans. Wireless Commun.*, vol. 18, no. 8, pp. 4003–4016, Aug. 2019.

[4] R. Bai, Q. Wang, and Z. Wang, "Asymmetrically clipped absolute value optical OFDM for intensity-modulated direct-detection systems," *J. Lightw. Technol.*, vol. 35, no. 17, pp. 3680–3691, Sep. 2017.

[5] M. S. A. Mossaad, S. Hranilovic, and L. Lampe, "Visible light communications using OFDM and multiple LEDs," *IEEE Trans. Commun.*, vol. 63, no. 11, pp. 4304–4313, Nov. 2015.

[6] R. Bai and S. Hranilovic, "Absolute value layered ACO-OFDM for intensity-modulated optical wireless channels," *IEEE Trans. Commun.*, vol. 68, no. 11, pp. 7098–7110, Nov. 2020.

[7] H. Kazemi and H. Haas, "On the performance of single side-band OFDM for band-limited visible light communication," in *Proc. IEEE Int. Conf. Commun. Workshops*, Dublin, Ireland, 2020, pp. 1–6.

[8] S. D. Dissanayake and J. Armstrong, "Comparison of ACO-OFDM, DCO-OFDM and ADO-OFDM in IM/DD systems," *IEEE/OSA J. Lightw. Technol.*, vol. 31, no. 7, pp. 1063–1072, Apr. 2013.

[9] X. Zhang, Z. Babar, P. Petropoulos, H. Haas, and L. Hanzo, "The evolution of optical OFDM," *IEEE Commun. Survey Tuts.*, vol. 23, no. 3, pp. 1430–1457, Jul.–Sep. 2021.

[10] X. Huang, F. Yang, C. Pan, and J. Song, "Flexible NOMA-based NOHO-OFDM scheme for visible light communication with iterative interference cancellation," *Opt. Exp.*, vol. 29, no. 4, pp. 5645–5657, Feb. 2021.

[11] R. Bai and S. Hranilovic, "Layered antisymmetry-constructed clipped optical OFDM for low-complexity VLC systems," *Opt. Exp.*, vol 29, no. 7, pp. 10613–10630, Mar. 2021.

[12] S. Mazahir, A. Chaaban, H. Elgala, and M.-S. Alouini "Achievable rates of multi-carrier modulation schemes for bandlimited IM/DD systems," *IEEE Trans. Wireless Commun.*, vol. 18, no. 3, pp. 1957–1973, Mar. 2019.

[13] S. Hranilovic and D. A. Johns, "A multilevel modulation scheme for high-speed wireless infrared communications," in *Proc. IEEE Int. Symp. Circuits Syst.*, Orlando, Florida, USA, 1999, pp. 338–341.

[14] K. Asadzadeh, A. A. Farid, and S. Hranilovic, "Spectrally factorized optical OFDM," in *Proc. 12th Can. Workshop Inf. Theory*, Kelowna, BC, Canada, 2011, pp. 102–105.

[15] A. Mecozzi, C. Antonelli, and M. Shtaif, "Kramers-Kronig receivers," *Adv. Opt. Photon.*, vol. 11, no. 3, pp. 480–517, Sep. 2019.

[16] A. Mecozzi, C. Antonelli, and M. Shtaif, "Kramers-Kronig coherent receiver," *Optica*, vol. 3, no. 11, pp. 1220–1227, Nov. 2016.

[17] A. Mecozzi, "A necessary and sufficient condition for minimum phase and implications for phase retrieval," 2016, *arXiv:1606.04861*.

[18] X. Chen *et al.*, "Kramers-Kronig receivers for 100-km datacenter interconnects," *IEEE/OSA J. Lightw. Techn.*, vol. 36, no. 1, pp. 79–89, Jan. 2018.

[19] T. Harter *et al.*, "Generalized Kramers-Kronig receiver for coherent terahertz communications," *Nature Photon.* vol. 14, no. 10, pp. 601–606, Sep. 2020.

[20] S. Hranilovic, *Wireless Optical Communication Systems*, Springer-Verlag New York, 2004.

[21] C. E. Shannon, "A mathematical theory of communication," *Bell Syst. Tech. J.*, vol. 27, no. 3, pp. 379–423, 623–656, Jul. 1948.
[22] Q. Wang, C. Qian, X. Guo, Z. Wang, D. G. Cunningham, and I. H. White, "Layered ACO-OFDM for intensity-modulated direct detection optical wireless transmission," *Opt. Exp.*, vol. 23, no. 9, pp. 12382–12393, May 2015.
[23] M. Safari, "Efficient optical wireless communication in the presence of signal-dependent noise," in *Proc. IEEE Int. Conf. Commun. Workshop*, 2015, pp. 1387–1391.
[24] L. Chen, B. Krongold, and J. Evans, "Performance analysis for optical OFDM transmission in short-range IM/DD systems," *J. Lightw. Technol.*, vol. 30, no. 7, pp. 974–983, Apr. 2012.
[25] T. Fath and H. Haas, "Performance comparison of MIMO techniques for optical wireless communications in indoor environments," *IEEE Trans. Commun.*, vol. 61, no. 2, pp. 733–742, Feb. 2013.
[26] L. Zeng *et al.*, "High data rate multiple input multiple output (MIMO) optical wireless communications using white LED lighting," *IEEE J. Sel. Areas Commun.*, vol. 27, no. 9, pp. 1654–1662, Dec. 2009.
[27] R. J. Muirhead, *Aspects of Multivariate Statistical Theory*. New York, NY, USA: Wiley, 1982.
[28] S. Hranilovic and F. R. Kschischang, "Capacity bounds for power-and band-limited optical intensity channels corrupted by Gaussian noise," *IEEE Trans. Inf. Theory*, vol. 50, no. 5, pp. 784–795, May 2004.
[29] A. Lapidoth, S. M. Moser, and M. A. Wigger, "On the capacity of free-space optical intensity channels," *IEEE Trans. Inf. Theory*, vol. 55, no. 10, pp. 4449–4461, Oct. 2009.
[30] H. Elgala and T. D. C. Little, "SEE-OFDM: Spectral and energy efficient OFDM for optical IM/DD systems," in *Proc. IEEE 25th Annu. Int. Symp. Pers., Indoor, Mobile Radio Commun.*, Washington, DC, USA, pp. 851–855.
[31] D. Tsonev, S. Videv, and H. Haas, "Unlocking spectral efficiency in intensity modulation and direct detection systems," *IEEE J. Sel. Areas Commun.*, vol. 33, no. 9, pp. 1758–1770, Sep. 2015.
[32] F. Xiong, *Digital Modulation Techniques*, *2nd ed*. Norwood, MA, USA: Artech House, 2006.
[33] J. Wang, Y. Xu, X. Ling, R. Zhang, Z. Ding, and C. Zhao, "PAPR analysis for OFDM visible light communication," *Opt. Exp.*, vol. 24, no. 24, pp. 27457–27474, Nov. 2016.

Ruowen Bai (Graduate Student Member, IEEE) received the B.S. degree from Nankai University, Tianjin, China, in 2015 and the M.E. degree (with Hons.) from Tsinghua University, Beijing, China, in 2018. He is currently working toward the Ph.D. degree with McMaster University, Hamilton, ON, Canada. His research interests include engineering optimization, modulation and signal processing for wireless communications and visible light communications.

Steve Hranilovic (Senior Member, IEEE) received the B.A.Sc. degree (with Hons.) in electrical engineering from the University of Waterloo, Waterloo, ON, Canada, in 1997, and the M.A.Sc. and Ph.D. degrees in electrical engineering from the University of Toronto, Toronto, ON, Canada, in 1999 and 2003, respectively. He is currently a Professor with the Department of Electrical and Computer Engineering, McMaster University, Hamilton, ON, Canada, and is currently an Associate Dean (Academic). During 2010–2011 he spent his research leave as a Senior Member, Technical Staff in Advanced Technology for Research in Motion, Waterloo, ON, Canada. He is the author of the book *Wireless Optical Communication Systems* (New York:Springer, 2004). His research interests include free-space and optical wireless communications, digital communication algorithms, and electronic and photonic implementation of coding and communication algorithms. Dr. Hranilovic is a licensed Professional Engineer in the Province of Ontario and was awarded the Government of Ontario Early Researcher Award in 2006. In 2016, the title of University Scholar was conferred upon him by McMaster University. He was an Associate Editor for the *Journal of Optical Communications and Networking* and the Editor of the IEEE TRANSACTIONS ON COMMUNICATIONS IN THE AREA OF OPTICAL WIRELESS COMMUNICATIONS.